TECHNICAL ARTICLE

Microstructure and Tribological Performance of Laser Cladding Ti₂AlC Particle Reinforced Coatings on Ti6Al4V

Shi-Wei Hua, Ming Pang, Jie Chen, Jie Zhao, and Feng-Qin Ji

By applying the TC4-Ti₂AlC composite coatings to the Ti6Al4V substrate by laser, the wear resistance of the Ti6Al4V alloy was improved. Analysis was done on the composite coatings' microstructure, phase composition, microhardness, and tribological characteristics. According to the findings, coatings without defects can be created when Ti₂AlC content ranges between 5 and 15 wt.%. Furthermore, the coating without Ti₂AlC consisted of a α-Ti solid solution while coatings with Ti₂AlC included a α-Ti solid solution, hard phases of TiC and Ti₃Al, as well as a Ti₂AlC ceramic phase. During laser cladding, Ti₂AlC partially dissolved and turned into TiC and Ti₃Al, resulting in an average hardness of 371.61 ± 3.95 HV$_{0.5}$, 382.92 ± 3.61 HV$_{0.5}$, 388.91 ± 3.29 HV$_{0.5}$ for the coatings with Ti₂AlC weight fractions of 5, 10, and 15%, respectively. These numbers were about $1.16 \sim 1.22$ times the hardness of the titanium alloy matrix (320 ± 3.12 HV$_{0.5}$). Besides, the Ti₂AlC lubricant and hard phases act synergistically to bring composite coatings better performances in wear resistance and friction reduction compared to the pure TC4 coating. The lowest coefficient of friction (0.382) (COF) and the greatest wear resistance (8.87×10^{-5} mm³/N m) were obtained at the composition of TC4-10wt.%Ti₂AlC; more particularly, the wear resistance at TC4-10wt.%Ti₂AlC was 1.2–2.1 times that of pure TC4 coating. The principal causes of wear in a pure TC4 coating are adhesive wear and oxidation, however, these wear processes shift to minor abrasive wear and oxidation when assisted by oxide coatings, Ti₂AlC lubricant, and TiC, Ti₃Al hard phases.

1. Introduction

An important component of the new transmission mechanism is the gear (Ref 1-3). For this reason, the strength and efficiency of gears is crucial. Since gears are responsible for transmitting power, they are subjected to extreme conditions throughout service, including high levels of alternating stress, contact stress, powerful impact force, and friction force (Ref 4-6). As the number of hours spent maintaining gears increases, new forms of failure manifest throughout the service phase. Extreme wear also causes a fast decline in tooth surface morphology, exacerbating failure. As a result, surface wear is the most critical failure in gear transmission. To address issues with gear surface failure, a protection surface must be implemented on its surface to improve the gear's anti-wear performance. Currently, TC4 alloy is the preferred material to manufacture the gear teeth, but the alloy itself is not resistant to wear (Ref 7). Currently, the traditional surface strengthening treatment methods commonly used at present mainly include induction heating quenching, carburizing quenching, nitriding treatment, laser quenching, etc. (Ref 8-10). Each technique has its own restrictions on what materials may be used, how thick layers can be deposited, how much force can be used to connect, and how much deformation can be applied to the final shape. Laser cladding technology, however, can offer innovative processing methods for crucial part repair and environmentally friendly remanufacturing, offsetting these shortcomings.

Adding a hard phase and a self-lubricating phase to a laser-wrapped protective coating for the surface of titanium alloy are the two most common approaches. However, directly adding the hardness phase, due to the difference in the thermophysical parameters of the hard phase, the cladding layer and the base material, leads to a relatively high crack sensitivity. Direct addition of lubricating phase, as the lubricating phase generally has low hardness, inappropriate lubricating phase will cause the hardness of the clad layer to decrease, thus reducing the anti-wear performance of the clad layer. Directly incorporating an optimal lubrication phase into the coating increases its wear resistance, moreover, a part of the lubricating phase decomposes at high temperature and generates hard phase in situ, thus improving the wear resistance and self-lubricating function of the clad layer.

Recently, scholars have started to focus on creating self-lubricating coatings by laser cladding. Not only lasers have a high-energy density, but also their paths can be precisely

Shi-Wei Hua, School of Transportation Science and Engineering, Civil Aviation University of China, Tianjin 300300, People's Republic of China; Ming Pang, College of Aeronautical Engineering, Civil Aviation University of China, Tianjin 300300, People's Republic of China; Jie Chen and Jie Zhao, Inner Mongolia Metallic Materials Research Institute, Ningbo, People's Republic of China; and Feng-Qin Ji, College of Aeronautical Engineering, Civil Aviation University of China, Tianjin 300300, People's Republic of China; and State Key Laboratory of Solid Lubrication, Lanzhou Institute of Chemical Physics, Chinese Academy of Sciences, Lanzhou 730000, China. Contact e-mails: pangming1980@126.com and chenjie0903@hotmail.com.

controlled. Fan et al. (Ref 11) investigated laser cladding of nickel-based/MoS_2 self-lubricating coatings on titanium alloy substrates and showed a good association between MoS_2 concentration and alloy hardness and wear resistance. The friction coefficients of the cladding layer dropped as well. However, as the MoS_2 content rose, covering flaws, such as rips and holes became more prevalent, resulting in poor homogeneity of the microstructure. The laser cladding process was used by Wang Pei et al. (Ref 12) to apply a self-lubricating layer of h-BN on titanium alloy substrates, h-BN showed very poor wetting capabilities in the metal matrix under low laser power. In addition, h-BN has a low density (2.27 g/cm^3), allowing it to float on the surface of the melt pool and spread out nonuniformly. When the laser power was low, h-BN demonstrated very poor wetting properties in the metal matrix. Additionally, the density of h-BN is low (2.27 g/cm^3), making it float on top of the melt pool and distribute heterogeneously. Furthermore, as the laser power rose, the substrate may melt and dilute in great amounts, inhibiting the h-BN self-lubricating phase from floating up. Moreover, the coating demonstrated a large dilution rate and low hardness. To demonstrate that MoS_2 was partially dissociated due to its low melting point of 1185 °C, Xu et al. (Ref 13) constructed a MoS_2/TiC/Ni-based composite cladding over 1045 low-carbon steel. Such dissociation will negatively affect the lubricating properties of this coating. Yang et al. (Ref 14) prepared 30wt.% WS_2 with NiCr-Cr_3C_2 coating by laser cladding. WS_2 and CrS were only present in modest amounts, according to x-ray diffraction studies, and they both degraded and oxidized in the presence of high-energy beam radiation. By laser cladding on aluminum alloy substrates, Podgornik B et al. (Ref 15) created h-BN self-lubricating coatings. They found that aside from the low density, h-BN has a very poor wettability in the metal matrix. Due to the coating's tendency to float on top of the molten pool, achieving homogenous distribution would be challenging. With the aid of Ag and MoS_2, Torres H et al. (Ref 16) created nickel-based self-lubricating coatings. Although the anti-friction and wear resistance properties significantly improved in all specimens, Ag diffusion in the coating shortened the coating service life. As can be seen from the studies above, numerous solid lubricants may be used, such as graphite, h-BN, sulfides (MoS_2, WS_2, etc.), fluorides (CaF_2, BaF_2, etc.), and soft metals (Ag, Cu, Sn, etc.) (Ref 17, 18). However, the preparation of lubricating coatings by laser cladding still faces challenges (Ref 19). Firstly, since the self-lubricating phase, the matrix phase, and the reinforcing phase of the coating vary in their thermal properties, cracks are prone to occur. Secondly, density differences between the self-lubricating phase and other substances in the coating may result in the former floating or sinking. Thirdly, the self-lubricating phase tends to oxidize, decompose and splash under a high-energy laser.

To overcome the shortcomings of these traditional solid-lubricating materials. MAX-phase Ti_2AlC was developed. Ti_2AlC is a ternary layered ceramic MAX-phase compound that exhibits both ceramic and metallic properties, thereby demonstrating significantly higher compatibility with titanium alloy substrates and the capability of crack healing when integrated with the substrates (Ref 20–24). MAX phases simultaneously possess high-temperature resistance, corrosion, oxidation and thermal shock resistance (Ref 25). Not only does the lubricity of ceramic Ti_2AlC reflect its role during laser cladding, but so does the material's capacity to break down into other elements and be used to create hard phases in situ.

Furthermore, Ti_2AlC has a laminar structure, which brings good lubricating properties during wear (Ref 26–30). In addition, due to the layered nature of the structure, no lubrication or cooling is required when processing specimens, and these capabilities offer great potential for MAX phase applications in extreme friction environments (Ref 31). Specifically, the Ti6C octahedral layer is divided by a single layer of atomic Al that is completely walled up in only two dimensions that has a weak bond to Ti in a way similar to a graphite layer, resulting in a laminar structure with self-lubricating properties (Ref 32–34). However, the previous study found it challenging to maintain a stable in situ creation of Ti_2AlC under preparation conditions. Because of this, the direct addition of Ti_2AlC powder was chosen as the approach to guarantee the desired amount of Ti_2AlC and fulfill all specifications. Furthermore, to improve the coating-substrate compatibility, TC4 powder was selected as the toughened phase. In engineering, self-lubricating area is only a thin layer on the coating surface (Ref 35). And a coating is considered damaged if it wears to a depth of more than 30 μm. For high wear resistance on the gear surface, a coating enriched with self-lubricating Ti_2AlC and hard phases more than 30 μm region of the coating surface is highly desirable.

MAX-phase as a solid-lubricating material in laser cladding is still under investigation. Particularly, Peter Richardson (Ref 36) was the first to synthesize MAX-phase Ti_2AlC in situ by laser cladding. Although MAX-phase coating is not novel as a concept, a lot of work has been performed to obtain dense, pure, and well-bonded coatings for industrial applications. Mitun Das (Ref 37) applied SiC powder to a titanium alloy substrate by laser cladding to enhance the mechanical and wear properties of the coating, but the Ti_3SiC_2 target phase was not detected by x-ray diffraction. Xin et al. (Ref 38) revealed the difficulties during the preparation of MAX-phase coatings by laser cladding in detail. Particularly, the maximum phase prepared by laser cladding is not the main crystalline phase of the coating, and laser cladding can hardly produce MAX-phase coatings with a high purity regardless of the preparation procedure. Since the anti-wear performance of the coating is influenced by Ti_2AlC decomposition under laser irradiation, a small amount of Ti_2AlC will affect the coating's resistance to wear, and a large amount of Ti_2AlC will affect the forming quality of the coating, this study aimed to investigate the regulation of coating performance with different Ti_2AlC contents and obtained, the optimal amount of Ti_2AlC addition, which is of significant supportive value for the optimization of the self-lubricating coating process in engineering.

2. Materials and Methods

Commercial TC4 alloys (100 × 50 × 10 mm) were chosen as the substrate material. TC4 (99% purity, 70–120 μm, BULWARK, China) and Ti_2AlC (99% purity, 20 μm, Warwick Rekor Metal, China) powders were used as the cladding material, the melting point of MAX phase Ti_2AlC is 2000 °C and the density is 4.11 g/cm^3, and their SEM figures are shown in Fig. 1. Specifically, Ti_2AlC powders had a clearly layered structure, which would bring certain self-lubricating properties to the coating. Besides, the self-lubricating phase Ti_2AlC should be added at an appropriate amount so that the coating can be fabricated with defect-free and excellent comprehensive
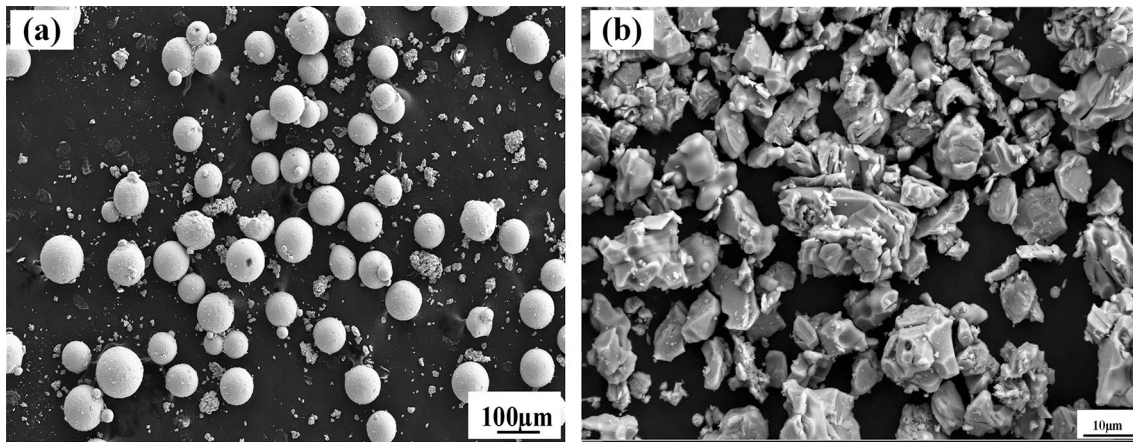
Fig. 1 Morphologies of laser cladding powders: (a) TC4 powder; (b) Ti$_2$AlC powder

Table 1   Chemical makeup of laser cladding powder

Number	Powder composition, wt.%
Sample 1	100TC4
Sample 2	95TC4 + 5Ti$_2$AlC
Sample 3	90TC4 + 10Ti$_2$AlC
Sample 4	85TC4 + 15Ti$_2$AlC

Table 2   Chemical composition of the TC4 powder (wt.%)

Al	Fe	C	N	V	Ti
6.37	0.05	0.01	0.01	4.06	Bal

performance. Furthermore, the cracks begin to develop in the coating, and the toughness of the coating decreases with more than 15wt.% Ti$_2$AlC through extensive pre-experiments. Similar results were observed in the study by Ai (Ref 39). Therefore, weight fractions of Ti$_2$AlC in the composites were fixed at 0, 5, 10 and 15wt.% to find the optimal one (see Table 1). The TC4 powder was selected as the self-fusing alloy, in which the Ti element is provided and the incompatibility between the coating and the substrate could be reduced. Besides, as a MAX-phase material, Ti$_2$AlC can generate protective films made up of Al$_2$O$_3$ and TiO$_2$ under friction wear, thereby being a self-lubricator that prevents further oxidation of Ti$_2$AlC. The powdered TC4 has the chemical makeup shown in Table 2. Before laser cladding, raw powders were mixed with a V-18 planetary ball (Changzhou Fanzhong Drying Equipment Company, China) mill for 10 h to ensure homogeneity. Silicon carbide sandpapers with mesh sizes ranging from 400 to 2000 were used to polish the sample's surface and remove the metal oxide. The next experimental step was washing the polished substrate samples with anhydrous ethanol. Particularly, the laser power should be optimum to prevent Ti$_2$AlC decomposition at high temperatures, improve the coating's bonding strength at the coating's interface and smooth out the coating's granules. In addition, the quick solidification structure of the clad layer is fine and homogeneous due to the laser cladding process. A relatively fast laser velocity is recommended to improve the coating's overall performance. Therefore, the coatings were fabricated with a laser cladding system (Nd: LSJG-GQ-6000M3, China) at a power of 2.4 kW, a scanning speed of 0.015 m/s, a spot diameter of 3.5 mm, an overlap rate of 50%, and a powder feeding rate of 10 g/min. Argon at a flow rate of 8 L/min was used to protect the molten pool from oxidation during laser
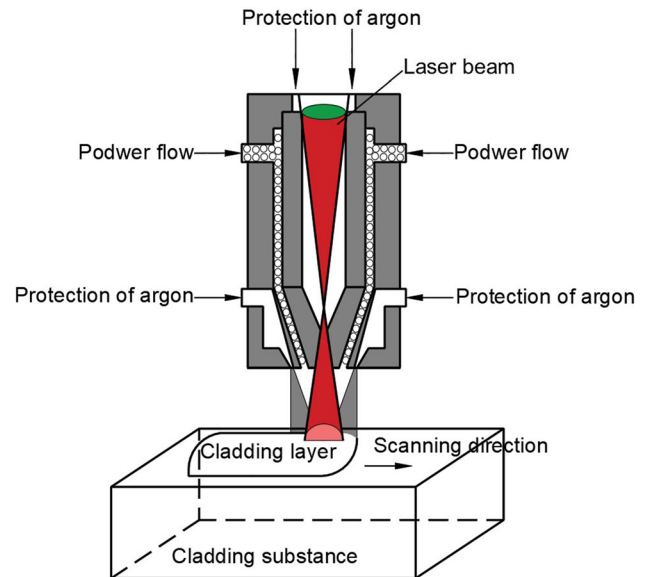

Fig. 2 The schematic diagram of the coaxial powder feeding

cladding. The powder was projected coaxially onto the laser beam through a coaxial nozzle. The coaxial powder feeding method and the laser cladding paths are described in Fig. 2 and 3. The distance between the deposition nozzle and the substrate plate is 20 mm, and preparation of single-layer cladding layers using laser cladding.

Afterward, penetration tests were conducted on the composite coating. Firstly, clean the surface of the coating with detergent, secondly, spray the penetrant evenly on the surface of the coating and leave it for 5–10 min, then remove the
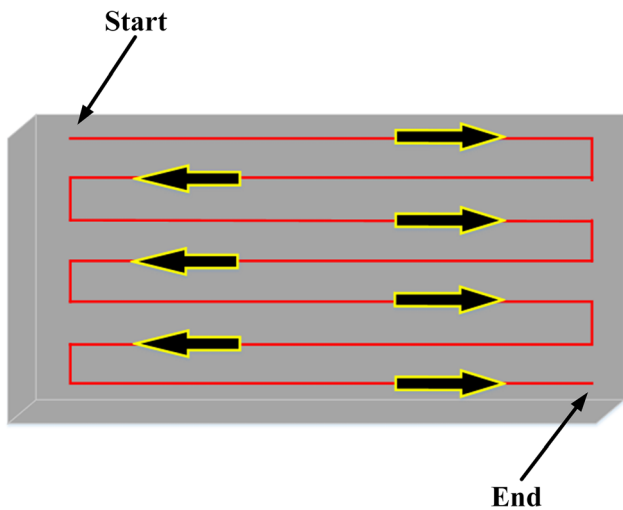
Fig. 3 The scanning path

Fig. 4 Schematic diagram of hardness measurement path

remaining penetrant on the surface with detergent, and finally spray the developer on the surface of the coating and wait for the result.

The metallographic samples were cut using a wire-cut machine (DK7740D, China) and then positioned vertically for scanning after the laser cladding experiment. Metallographic sandpapers (numbers 60 through 2000) and a polish-grinding machine (Laizhou Wei Yi Test Equipment Manufacturing Company, China) were used to smooth the specimens' cross sections. Then, the clad layer was etched with etchants (HNO_3: HF: H_2O = 1:2:7), and the dwell time of etch was 10–30 s.

XRD tests were performed on the coatings surface, coatings on test specimens were analyzed for their microstructure and elemental distributions using a scanning electron microscope (SEM; Gemini SEM 300 ZEISS) with energy-dispersive spectroscopy (EDS). Cu Kα radiation at 45 kV, 200 mA, a scanning rate of 8°/min, and a 2-scanning range of 10°–100° were used in an x-ray diffraction (XRD, Rigaku D/max-2500/ PC Japan) instrument to determine the phases present in the specimens.

A digital micro hardness tester model 401MVSD (Bong Yi Precision Gauge Shanghai Company, China) was used to measure the hardness of coated cross sections in the depth direction under 500 g for 10 s (Fig. 4). Every 100 μm of the coating's thickness and the underlying substrate's thickness were measured for hardness. And at the same height, three measurements were taken.

Using a frictional wear tester model M-2000, the dry slide friction and wear of 10 × 10 × 10 mm specimens were determined (Hen Xu, Jinan, China). The experimental principles and parameters are described in Fig. 5 and Table 3. The friction wear surfaces were ground by #60 to #2000 metallographic sandpapers before the measurements. The wear couple ball made of Gcr15 steel had a diameter of 6 mm, and wear volume measurements were performed using a 3D optical profiler(UP-Lambda, Atech Instrument Technology, American). The following equation was used to determine the matrix and cladding layer wear rates: (Ref 40).
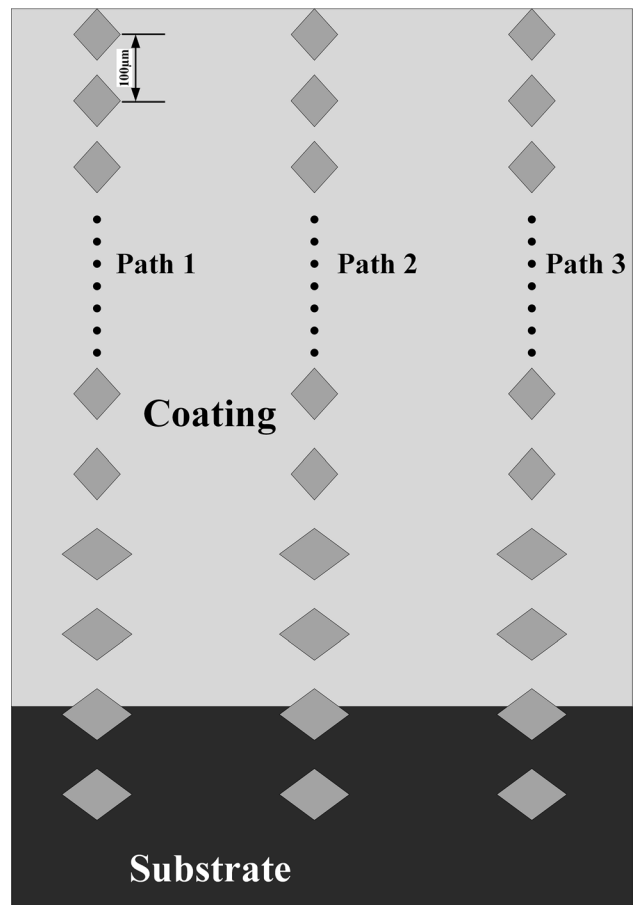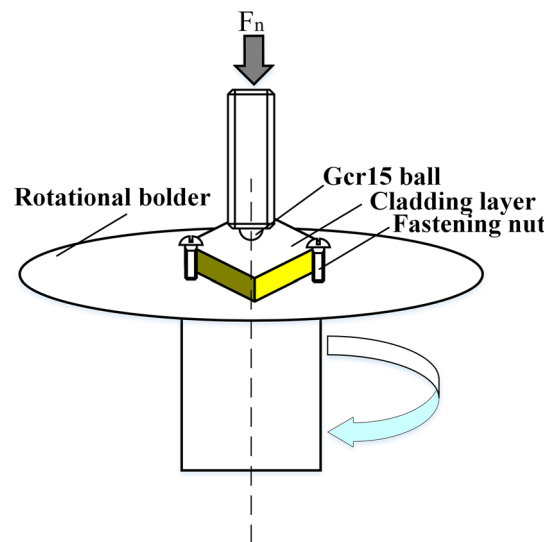
$$W = {\Delta V}/{F \times S}$$

Fig. 5 A schematic diagram of friction and wear principles

Herein, the Wear rate (in mm^3/Nm) is denoted by W, the volume of clothing worn is denoted by the letter ΔV (mm^3), a normal force (F) is defined by the product of the sliding distance (S), and the normal force (N) (m). Tests were completed three times per sample to measure the friction coefficient and wear rate.

Table 3 Parameters of the wearing test

Wear time, min	Load, N	Rotation speed, r/min	Rotation radius, mm	hardness of wear couple balls, $HV_{0.5}$
40	20	300	1.5	900
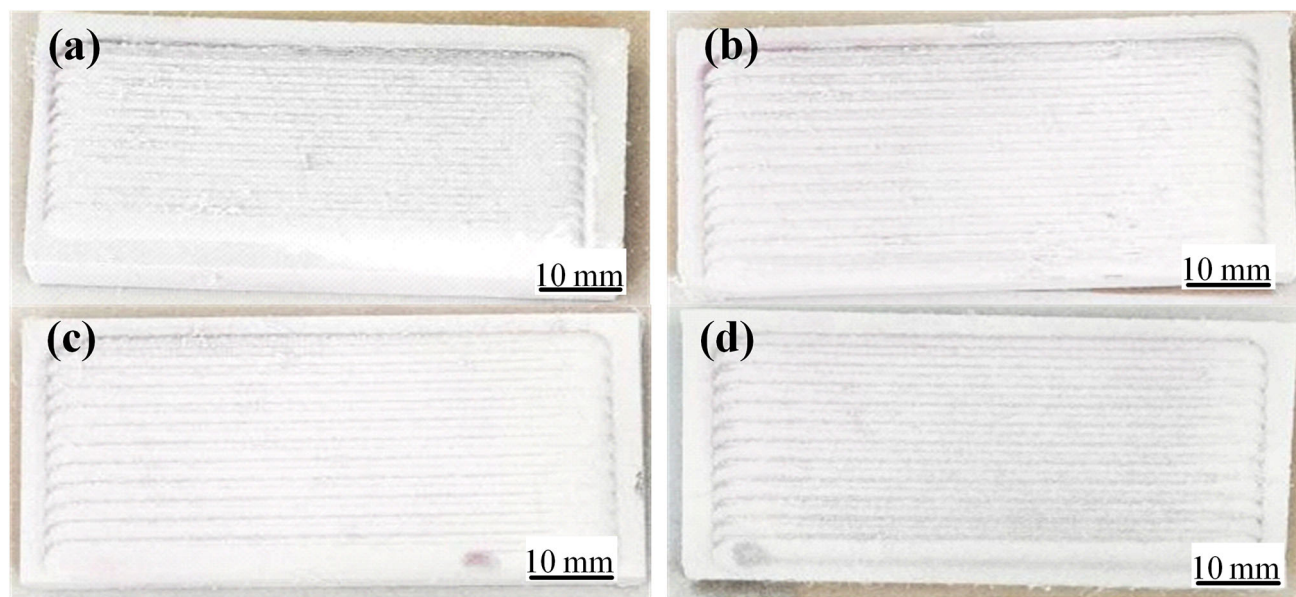
Fig. 6 Penetration testing of the coatings. (a) 0wt.%Ti_2AlC; (b) 5wt.%Ti_2AlC; (c) 10wt.%Ti_2AlC; (d) 15wt.%Ti_2AlC

After putting the specimens through a series of friction and wear tests, their chemical makeup was analyzed using an x-ray photoelectron spectrometer (AXIS SUPRA, China). Test at the location of the wear trace on each specimen. Initially, the binding energy was calibrated using contaminated carbon exhibiting the O1s peak at 530 eV.

3. Results Discussion and Analysis

3.1 Influences of the Ti_2AlC Content on the Coating's Macroscopic Morphology

The penetrant test (PT) is a non-destructive technique that detects surface-clacking faults in materials (Ref 41). Figure 6 shows the PT data for various Ti_2AlC concentrations in TC4 coatings, and all four sample coatings were observed without pores or cracks. The formation of pores is closely related to the fluidity of the melt pool. Since the main material of the cladding layer is TC4 powder, which has good fluidity, while cladding is being done, the gas into the pool is escaped from the melt pool through strong convection, and the formation of cracks is closely related to the matching of the thermal parameters of the cladding layer and the substrate. The TC4 selected for the cladding layer is the same as the thermal parameters of the substrate. Furthermore, the coefficient of thermal expansion is close to Ti_2AlC, resulting in cracks-free in the cladding layer.

Figure 7 displays the macro morphology of the coating cross section. The coatings securely adhered to the substrate, as evidenced by the presence of a defect-free fusion line at the cladding/substrate interface. The coatings with Ti_2AlC contents of 0wt.%, 5wt.%, 10wt.%, and 15wt.% had thicknesses of approximately 1.670 ± 0.023, 1.566 ± 0.019, 1.530 ± 0.026, and 1.528 ± 0.018 mm, respectively, suggesting as the Ti_2AlC content increases, the thickness of the cladding layer decreases, the high melting point (3000 °C) of Ti_2AlC causes it to require more energy during laser cladding, which makes less melting of TC4 and a lower thickness of the clad layer with the same laser energy. As the good fluidity of TC4 alloy powder as well as the powder's good compatibility with the substrate, the coating with 0wt.% Ti_2AlC addition exhibited a straight flat bonding line between itself and substrate. Besides, Ti_2AlC addition also affected the fluidity of the molten pool. Therefore, with greater Ti_2AlC addition, the bonding line between the coatings and the substrate changed from a straight flat line to a waved curve.

3.2 Coatings' Physical Phase Analysis of Ti_2AlC Composition

Figure 8 displays the laser cladding coatings' x-ray diffraction patterns, the coating without Ti_2AlC consisted of a α-Ti solid solution while coatings with Ti_2AlC included a α-Ti solid solution, hard phases of TiC and Ti_3Al, as well as a Ti_2AlC ceramic phase. Furthermore, when the content of Ti_2AlC coating was 10wt.%, Ti_2AlC demonstrated the highest diffraction peak intensity, suggesting a great Ti_2AlC content. The Gibbs free energy (ΔGT) of possible reactions (2)-(3) was computed and used with the XRD data to reveal the production process of reinforcing phases in the coatings in great detail. The thermodynamic properties of the inorganic materials handbook
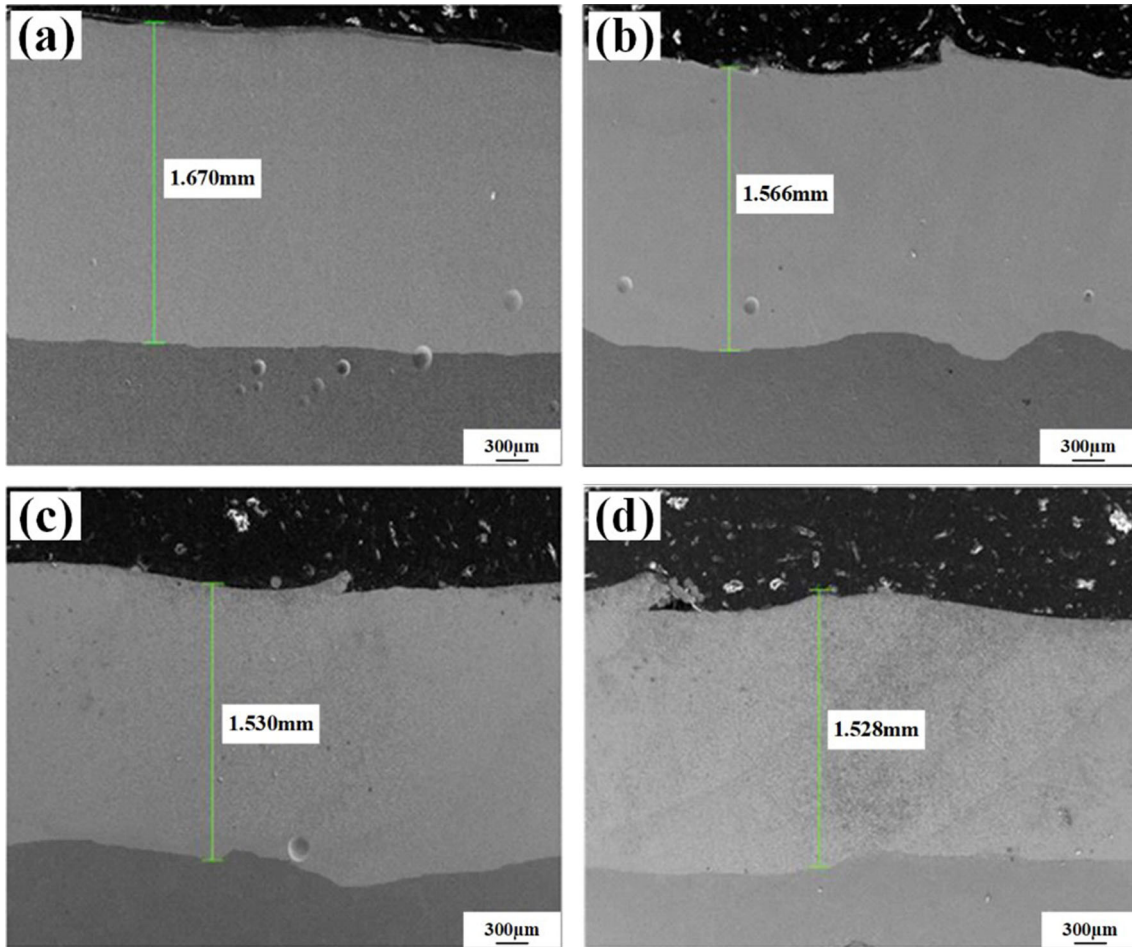
Fig. 7 Macro morphology of the coating cross sections with different Ti$_2$AlC contents; (a) 0wt.%Ti$_2$AlC; (b) 5wt.%Ti$_2$AlC; (c) 10wt.%Ti$_2$AlC; (d) 15wt.%Ti$_2$AlC
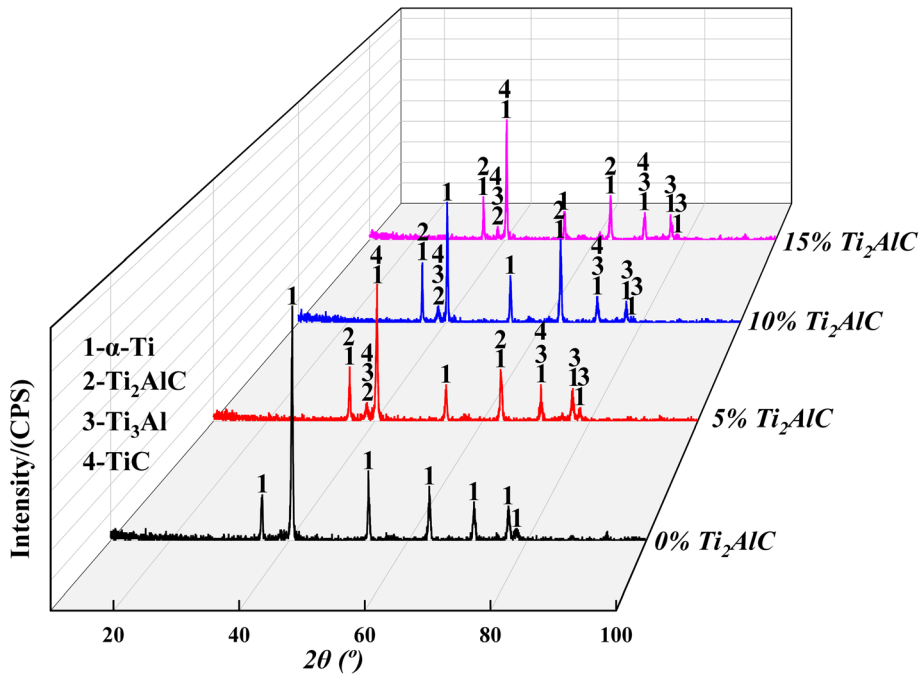

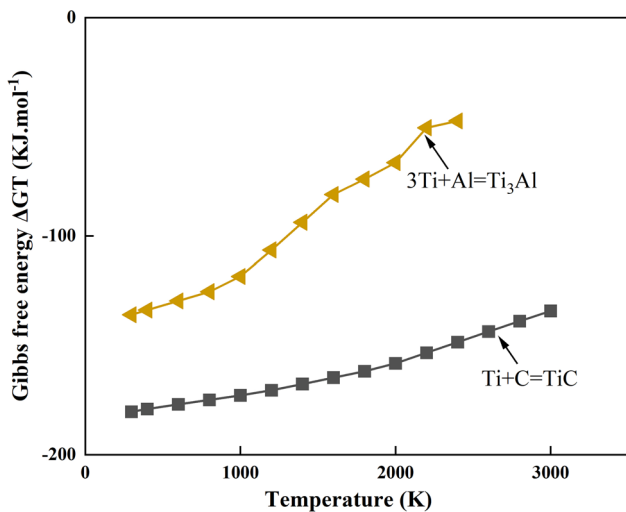**Fig. 8** The laser cladding coatings' x-ray diffraction patterns

Fig. 9 An estimate of the Gibbs free energy for reactions that may take place in the coatings

are used to determine material parameters for computations (Ref 42). Each reaction's Gibbs free energy is depicted in Fig. 9. If ΔGT (reaction $2-3$) < 0, then the anticipated carbide and boride compounds may develop in situ by spontaneous nucleation. Furthermore, TiC has a higher melting point than Ti_3Al and a greater $|\Delta GT$ (reaction 2)|, indicating that the TiC phase generated in situ is more stable. Because of this, the molten pool is initially used to precipitate TiC phases. Then, when the temperature is below its melting point, Ti_3Al starts to precipitate. From these aforementioned findings, Ti_2AlC self-lubricating coating is deduced to form during laser cladding by the following mechanism. Firstly, the powders and substrates experienced a gradual temperature rise under the direct laser irradiation and eventually turned into a molten pool. Simultaneously, Ti_2AlC partially dissolved to form TiC and Ti_3Al (formula 1). Subsequently, since carbon atoms had a stronger affinity with molten Ti atoms in the molten pool than aluminum ones, TiC was formed with higher priority than Ti_3Al. When the C element in the molten pool was exhausted, Ti_3Al started to appear (formulas 2 and 3).

$$Ti_2AlC \rightarrow TiC + Ti_3Al \qquad (Eq\ 1)$$

$$Ti + C \rightarrow TiC \qquad (Eq\ 2)$$

$$Ti + Al \rightarrow Ti_3Al \qquad (Eq\ 3)$$

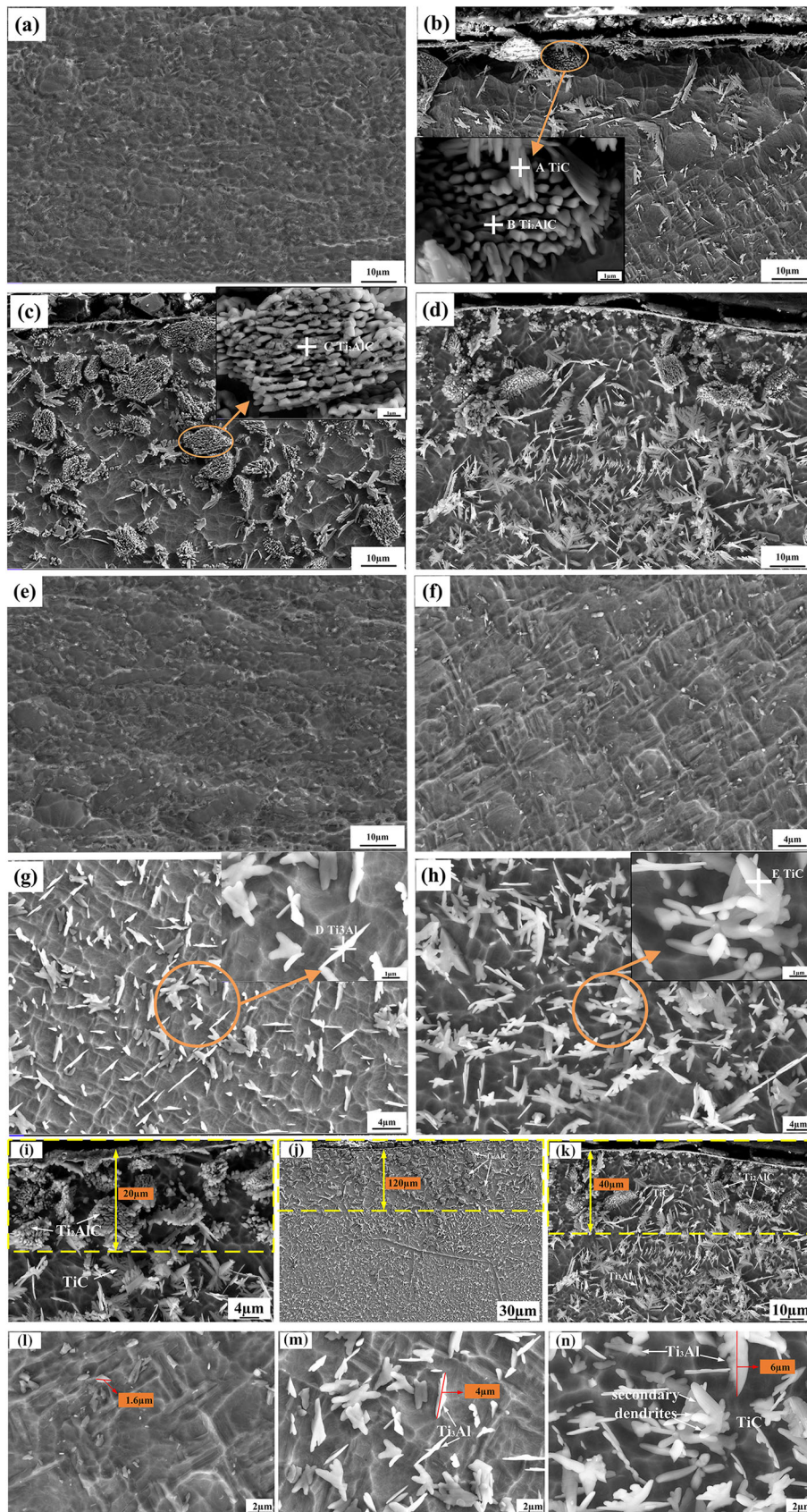### 3.3 Effect of Ti₂AlC Content on the Coating Microstructure

The scanning electron microscope pictures of the four coatings are shown in Fig. 10. Figure 10(a) and (e) shows the microstructures of the upper and middle parts of the coating without Ti_2AlC, which was mainly composed of α-Ti (Ref 43) columnar dendrites. Compared with the substrate, the α-Ti coating was finer and denser. This indicates that a fine, homogeneous, and swiftly formed coating structure may be created using laser cladding's rapid heating and cooling. Figure 10(b), (c) and (d), (f), (g) and (h) presents the microstructures of the upper and middle parts of the coatings with Ti_2AlC, which reveal significant changes in the composite

microstructure to small particle clusters (B, C) with a layered structure, dendrites (A, E), and rod-like crystals (D). Particularly, the small particle clusters with a layered structure were the most distributed and demonstrated the highest density when 10wt.% Ti_2AlC was added. Besides, the dendrites and rod-like crystals were gradually coarsening as the Ti_2AlC content went up. This can be explained as a result of reduced molten pool fluidity due to the addition of Ti_2AlC high-melting medium, which further negatively influenced the temporal and spatial uniformity of flow and heat transfer. Consequently, the temperature gradient G inside the molten pool increased, and the solidification rate R dropped. According to the solidification and crystallization theory (Ref 44-46), such changes in G and R may increase the shape factor for the solidified structure (Fig. 10l, m and n), leading to coarsening of the short rod-shaped and dendrite grains as the Ti_2AlC content rose and a rise of dendrite spacing from 1.6 μm to 6 μm. Moreover, As shown in Fig. 10(R), the generation of a large number of secondary dendrites also further illustrates that with the increase of Ti_2AlC content, the temperature gradient G in the molten pool further increases, so there is a wider undercooling zone, and the dendrites on the solid–liquid interface. The grains are able to grow deeper into the melt and obtain a greater degree of undercooling to form primary dendrites. When the composition of the side of the primary dendrite is too cold, branches grow on the side to form the secondary dendrite.

To identify the microstructure and phase composition of the coatings more clearly, high-magnification images of typical coating microstructures were obtained and their elemental compositions analyzed by EDS (Table 4). For example, a rough atomic ratio of 2:1:1 was observed among the constituent atoms of the tiny particle clusters (B, C). The dendrite crystals(A, E) contained only C and Ti elements in an approximate atomic ratio of 1:1. Finally, rod-like crystals (D) were composed of primarily Ti and Al, but the former has a much larger concentration compared to the latter. Along with the XRD results, these findings confirmed that the small particle clusters, cellular dendrites, and rod-like crystals were composed of primarily Ti_2AlC, TiC, and Ti_3Al, respectively. From Fig. 10(i), (j) and (k), it can be found that for Ti_2AlC contents of 5, 10, and 15wt.%, the certain depth on the surface of the coating enriched with the self-lubricating phase Ti_2AlC were 20 μm, 120 μm, and 40 μm, respectively. This can be explained as a result of Ti_2AlC powder migration to the top of the molten pool during laser cladding due to its low density (Ref 47). Meanwhile, the solidification rate at the molten pool bottom was lower than that at the top, resulting in lower Ti_2AlC contents at the bottom. Consequently, most Ti_2AlC powders migrated to the molten pool top and solidified and crystallized to form the upper surface of the cladding layer.

3.4 Effect of Ti₂AlC Content on the Coating Hardness

The hardness profile from the cladding layer to the matrix along the depth axis in Fig. 11(a). All four coatings had much greater hardness than the substrate. Figure 11(b) displays the typical substrate and coating hardness. Typically, a coating made of Ti_2AlC has a hardness of weight fractions of 0wt.%, 5wt.%, 10wt.%, and 15wt.% was 340.95 ± 3.41 $HV_{0.5}$, 371.61 ± 3.95 $HV_{0.5}$, 382.92 ± 3.61 $HV_{0.5}$, 388.91 ± 3.29 $HV_{0.5}$ higher than the substrate, respectively. When TC4 powder is cladded on the TC4 substrate, the coating hardness became slightly higher than the substrate. As for why the level

of difficulty suddenly shifted, consider the following: To begin, the laser cladding process causes fast heating and cooling, which swiftly solidifies the clad layer into a fine structure. Second, the melting pool had a high condensation rate, thus large alloying elements like V, Fe, and Al could not fully precipitate before being dissolved to fortify the solid solution. Furthermore, the coating hardness increased as the Ti$_2$AlC content rose, but the increasing extent was less than proportional. XRD analysis shows that laser cladding breaks down Ti$_2$AlC into hard phases like TiC and Ti$_3$Al, which become lodged in the coatings and aggregate at grain boundaries to stop dislocation movement and generate the second phase strengthening effect. Furthermore, as seen in Fig. 10(c) and (d), the

Table 4 Energy spectrum analyses of each point marked in Fig. 10 (at.%)

Point	Element composition		
	Ti	Al	C
A	52.77	1.15	46.09
B	50.93	21.72	27.35
C	62.41	16.85	20.74
D	77.52	20.53	1.95
E	54.23	1.98	43.79
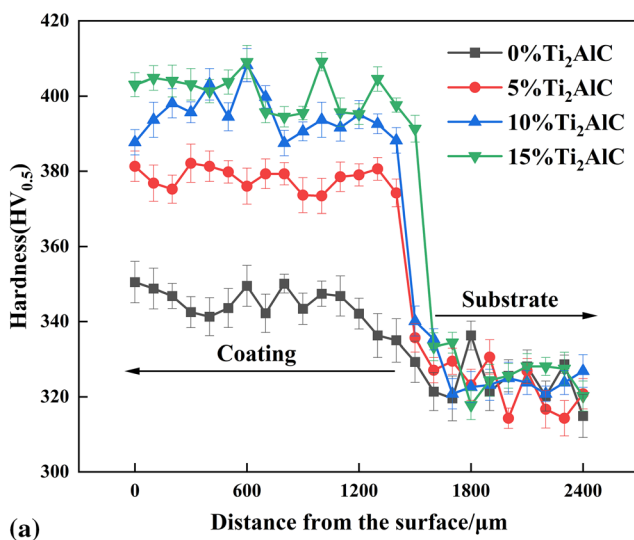
microstructure distribution shows that the addition of 15wt.% Ti$_2$AlC resulted in fewer ceramic precipitates than the addition of 10wt.% Ti$_2$AlC. This further confirms that at 10wt.% Ti$_2$AlC addition, more Ti$_2$AlC is retained in the coating. Therefore, processes for reinforcing grain boundaries and dispersion are both intended to increase the coating's hardness. When the content of Ti$_2$AlC was 10wt.%, XRD and EDS results demonstrated the maintenance of a large amount of Ti$_2$AlC, so the hard phases, such as TiC and Ti$_3$Al generated by decomposition did not increase proportionally. Because of the poor wettability between the matrix and Ti$_2$AlC when the addition of Ti$_2$AlC surpassed 10wt.%, Ti$_2$AlC agglomeration appeared, resulting in massive decomposition of Ti$_2$AlC during laser cladding. Similar results were observed in the study by Wang (Ref 48). Besides, these hard phases grew in grain size as the Ti$_2$AlC content rose, which would weaken the increase in coating hardness. Therefore, the increase in coating hardness values was less than proportional to the rise of Ti$_2$AlC content. Besides, the 0wt.%Ti$_2$AlC coating exhibited a small fluctuation in its hardness, which indicated a uniform grain size in the coating as confirmed by the microstructure observations. As Ti$_2$AlC was added, the fluidity of the molten pool dropped. Coatings made of Ti$_2$AlC have many variations in their hardness values because of the uneven flow of the molten pool, which caused the uneven distribution of the strengthening phase and grain.

3.5 Effect of Ti$_2$AlC Content on the Coating's Wear Properties

Figure 12 displays the friction coefficient curves of the coatings with different Ti$_2$AlC contents, and Fig. 13 displays the average friction coefficients of the four coatings were 0.486, 0.457, 0.382, and 0.415. Particularly, TC4-Ti$_2$AlC composite coatings demonstrated lower friction coefficients than the pure TC4 coating; besides, compared with pure TC4 coating, within the first three minutes of the friction and wear test, the 5wt.%Ti$_2$AlC coating demonstrated a relatively stable friction coefficient, which nevertheless increased and fluctuated violently in the later experimental stage. This may be explained
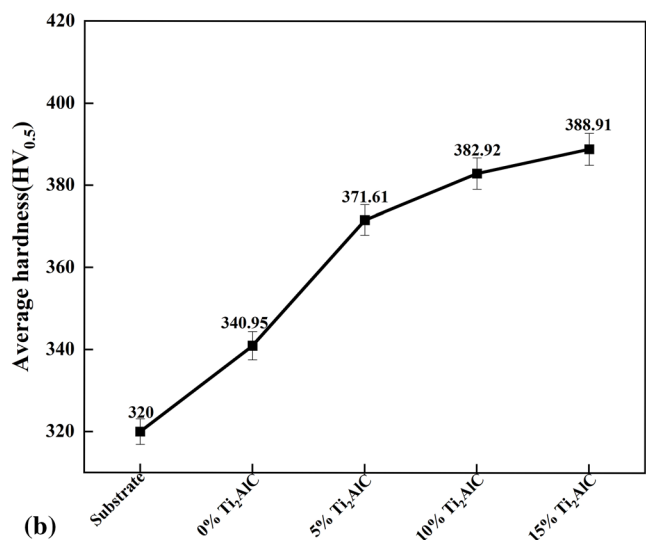

(a)

(b)

Fig. 11 The hardness of composite coatings with different Ti$_2$AlC contents. (a) The hardness distribution from the surface of the cladding layer to the substrate. (b) Average hardness of coatings and substrate
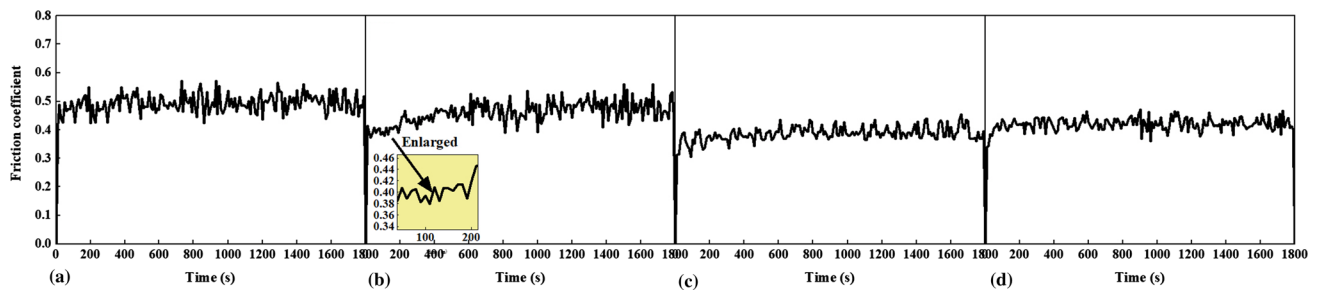
Fig. 12 The friction coefficients of the coatings with different Ti$_2$AlC contents. (a) 0wt.%Ti$_2$AlC; (b) 5wt.%Ti$_2$AlC; (c) 10wt.%Ti$_2$AlC; (d) 15wt.%Ti$_2$AlC
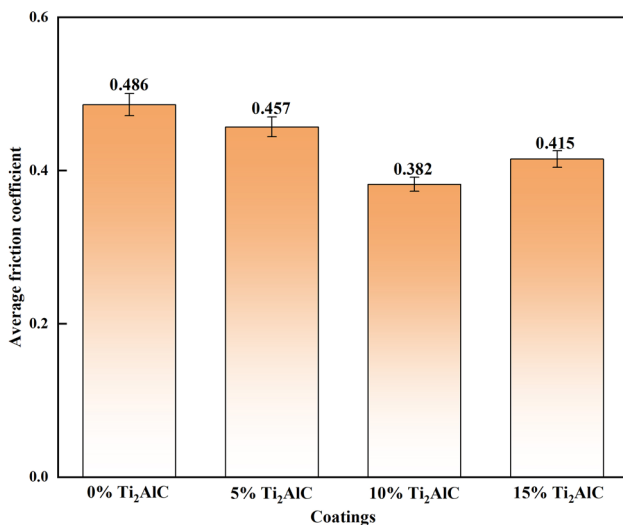

Fig. 13 Average friction coefficient of the Coatings

because a large amount of self-lubricating phase Ti$_2$AlC was distributed on the upper surface of the cladding layer, resulting in an uneven distribution of hard phases TiC and Ti$_3$Al. When the friction and wear experiments began, the solid self-lubricating phase was in contact with the grinding ball with a low friction coefficient. According to Fig. 10(m), the depth on the surface of the coating distribution the self-lubricating phase Ti$_2$AlC was no bigger than 20 μm. However, as the wear experiment continued, the grinding ball began to contact the depth on the surface of the coating that was more than 20 μm away from the initial coating surface. According to Fig. 14, the worn surface profile showed that the wear scar depth was 23.44 μm when the content of Ti$_2$AlC was 5wt.%. When the depth of the worn area exceeded 20 μm, few self-lubricating phases could be found, increasing the friction coefficient. In addition, the friction coefficients of the 10wt.%Ti$_2$AlC and 15wt.%Ti$_2$AlC coatings also fell significantly but with a stable variation. These coatings exhibited shallower wear scars with depths of 14.38 μm and 17.87 μm, respectively, with a large amount of Ti$_2$AlC distributed in the wear area. In order to further investigate the chemical composition information of the four coatings after the wear test, the XPS was carried out. Figure 15 showed the four coatings at the same position of wear scars under XPS photoelectron spectroscopy. O-Ti and O–Al bonds contributed to the appearance of two peaks in the O 1s spectra (E_b = 530, 532 eV) in the coatings. The spectra of Ti 2p displayed three peaks (E_b = 453.2, 458.5 and 464.5 eV) in the

coating without Ti$_2$AlC, which were associated with the Ti and TiO$_2$, and three peaks (E_b = 453.8, 458.5 and 464.5 eV) in the coatings with Ti$_2$AlC added. Moreover, the spectra of Al 2p displayed only peaking at a single Eb 74 eV in the coating without Ti$_2$AlC, which were associated with the Al$_2$O$_3$, and two distinct maxima, at Eb 71.7 eV and 74 eV in the coatings with Ti$_2$AlC added were found. Which were associated with the Ti$_2$AlC and Al$_2$O$_3$. Similar results were observed in the study by Wang (Ref 49). Where TiO$_2$, Al$_2$O$_3$ and Ti$_2$AlC were found in the 5wt.%Ti$_2$AlC, 10wt.%Ti$_2$AlC and 15wt.%Ti$_2$AlC coatings during the friction and wear process. Both oxides exhibited a similar lubricating effect as Ti$_2$AlC during the wear process, thereby reducing the coatings' friction coefficient. Air oxidation also made it simple to transform Ti and Al atoms into TiO$_2$ and Al$_2$O$_3$, respectively. Therefore, the coating's surface was quickly oxidized throughout the wear experiment, resulting in a thick oxide deposit. As grinding progressed, the oxide layer would be depleted and regenerated, eventually reaching a dynamic equilibrium condition. As shown in Fig. 12(c) and (d), the COF curve has entered a stable wear period, which is consistent with the oxide film's primary role of fixing and maintaining the coatings. A variety of coatings' wear rates are depicted in Fig. 16. Specifically, when the Ti$_2$AlC content was 0, 5, 10, and 15wt.%, the wear rate of the coatings was 25.46 × 10^{-5} mm^3/N·m, 22.35 × 10^{-5} mm^3/N·m, 8.87 × 10^{-5} mm^3/N·m, and 12.13 × 10^{-5} mm^3/N·m, respectively. The 10wt.% Ti$_2$AlC coating exhibited the highest wear resistance among all coatings, which was 2.1 times that of 0wt.% Ti$_2$AlC coating. Possible explanation: lubricants made of Ti$_2$AlC. The hard phases comprised the second phase of the coating's reinforcement and had a consistent role. One finding from earlier studies is that the coating has a higher hardness and resistance to wear because Ti$_2$AlC and the hard phases created by its disintegration are present there. However, dislocation slip along the basal plane was commonplace in Ti$_2$AlC powder due to the poor covalent binding strength of Al and Ti between the graphite-like layers. The delamination of the Ti$_2$AlC basal surface and the rise in dislocation slip energy resulted from the bending of the structure in a direction perpendicular to the base surfaces when subjected to an external strain.

In addition, compared with 5wt.% Ti$_2$AlC coating or 15wt.% Ti$_2$AlC coating, the 10wt.% Ti$_2$AlC coating exhibited the highest wear resistance. The following reason may be explained as: the 10wt.% Ti$_2$AlC coating has low frictional resistance, medium toughness, and moderate hardness, and a suitable assemblage of high hardness, low coefficient of friction, and toughness could contribute to the improvement of the wear resistance.
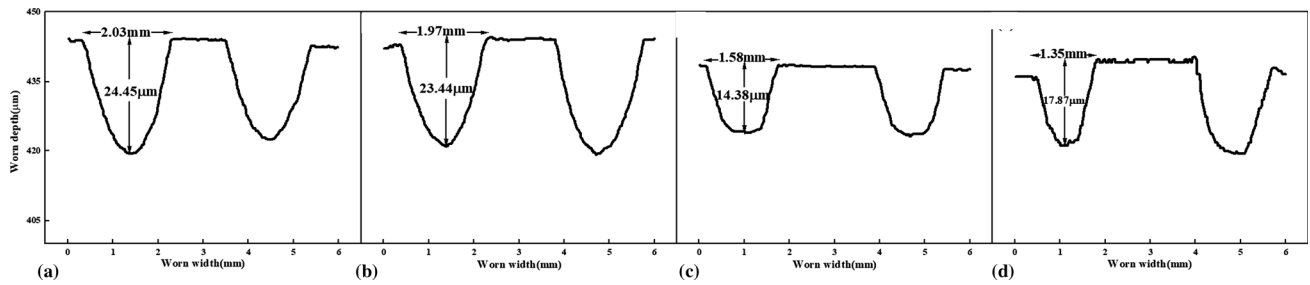
Fig. 14 Wear surface characteristics of varied Ti_2AlC content cladding layers. (a) 0wt.%Ti_2AlC; (b) 5wt.%Ti_2AlC; (c) 10wt.%Ti_2AlC; (d) 15wt.%Ti_2AlC
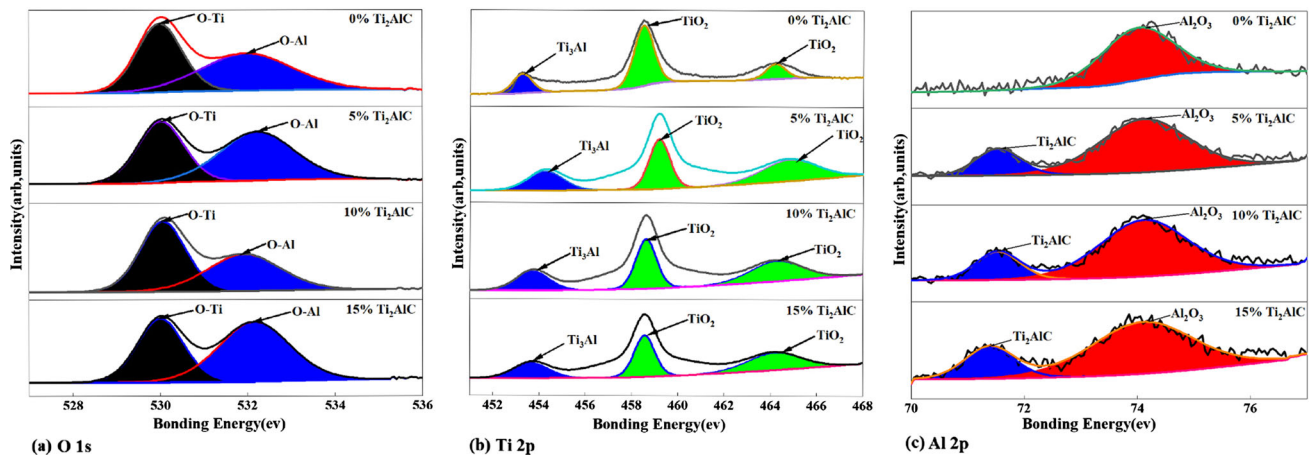

Fig. 15 Cladding layers' XPS core-level spectra at various Ti_2AlC concentrations. (a) O1s; (b) Ti2p; (c) Al2p
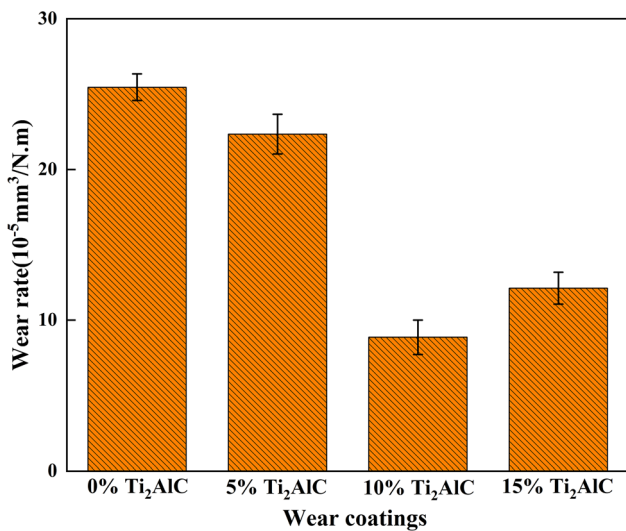

Fig. 16 Diagram demonstrating the rate of wear of several Ti_2AlC-containing cladding layers

3.6 Effect of Ti_2AlC Contents on the Coating's Wear Mechanism

SEM was used to characterize the wear morphology of the four coatings to explain the wear rate variations in detail (Fig. 17). When the Ti_2AlC content was 0wt.%, the worn coating surface was full of typical plastic deformations and furrows, packed with microscopic particles, which was attributed to the exfoliation-induced creation of huge bulk debris. In the wear experiment, the frictional pair was repeatedly squeezed and ground, causing the bigger pieces of debris to become smaller particles. Large blocks made up the majority of the wear debris, with some surface-found particles being somewhat agglomerated (Fig. 17a). Due to the coating's poor hardness, the GCr15 balls stuck to its surface throughout the wear process and tore or squeezed it out, leaving furrows in its wake. Furthermore, three-body wear occurred on the coating surface, the significant COF value of the coating was accompanied by repeated squeezing or grinding of the big pieces of flaking wear debris into smaller pieces (0.486). As a result, abrasive wear, plastic deformation, and adhesive wear made up the coating's wear mechanism. When the Ti_2AlC content was 5wt.%, furrows, wear debris (A), and plastic deformations were still present on the coating surface, but the furrows became shallower compared to those in the pure TC4 coating. The hardness of the coating and the adhesion resistance to the grinding ball were both raised because of the effects of the strengthening of α-Ti in solid solution and the distribution of the hard phases. The coating's ability to withstand plastic deformation was improved simultaneously, giving it outstanding abrasion resistance. Compared to pure TC4 coating, the higher area of the coating contained Ti_2AlC and the hard phases created by its disintegration, improving the surface hardness and wear resistance. After extensive use, the coating's surface developed abrasive pits and lumps as well as granular wear
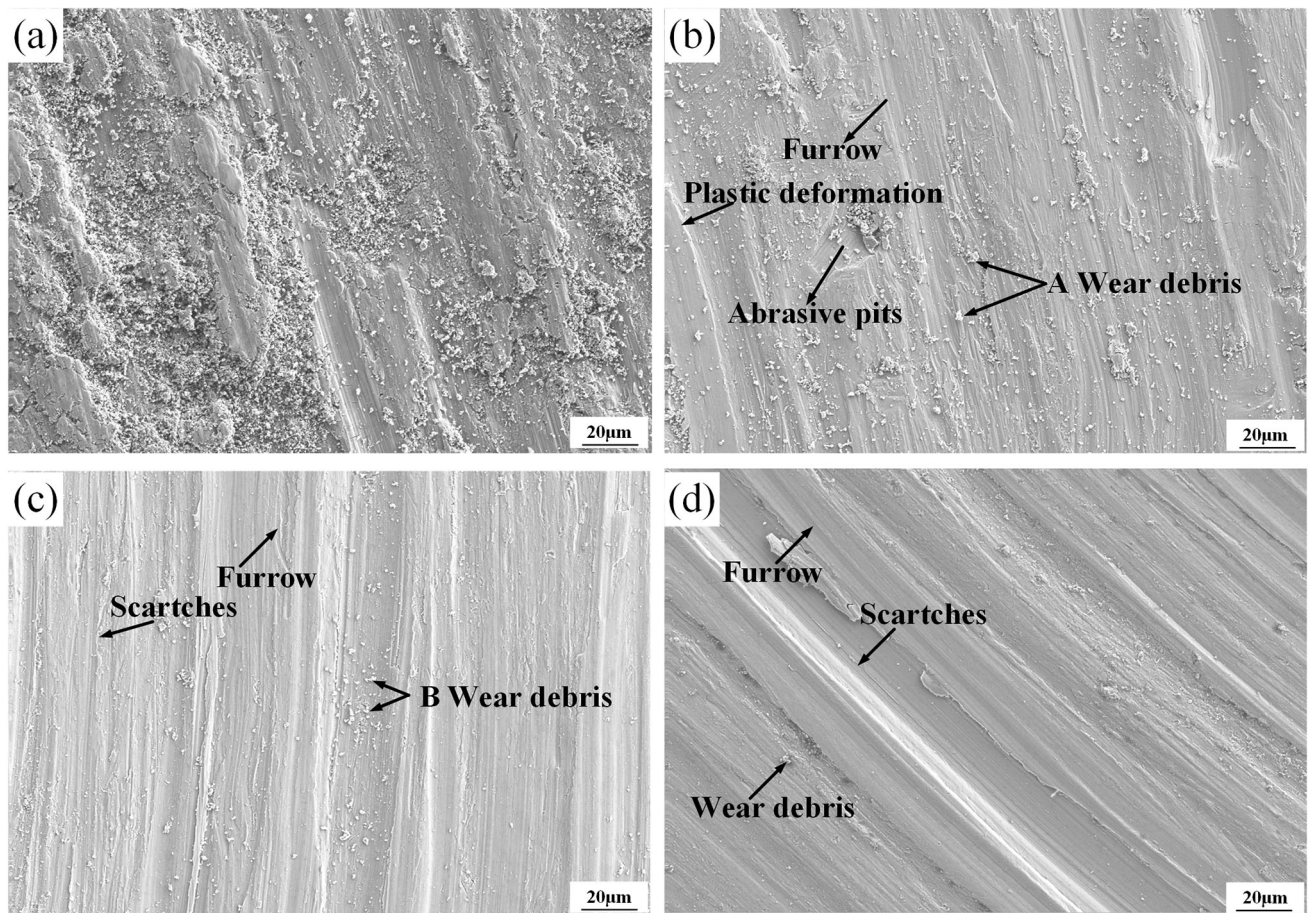
Fig. 17 SEM images of the cladding layers' worn surfaces with varying Ti_2AlC concentrations. (a) 0wt.%Ti_2AlC; (b) 5wt.%Ti_2AlC; (c) 10wt.%Ti_2AlC; (d) 15wt.%Ti_2AlC

debris (Fig. 17b), which may be attributed to the Ti and Al elements participating in an oxidation process with oxygen from the atmosphere (Ref 50). The heat produced during the friction process led to a layer of soft and thin oxide coating. On the worn surface, however, the oxide layers are insufficient. The scrap was also prone to breaking, and a sizable portion of its surface area dropped off, creating big chunks of debris. The flaking debris could behave as wear particles that are abrasive and aggravate the wear. It was challenging to generate a lubricating layer during wear because there weren't enough Ti_2AlC lubricating phases. Adhesive wear was primarily the wear mechanism. Plowing, wear depth, and plastic deformations were all greatly decreased when the Ti_2AlC concentration was 10 or 15 wt.%, compared to the pure TC4 coating (Fig. 17c and d). In addition, compared to the pure TC4 coating, peeling off and plastic deformations were reduced, and no visible groove was seen. Describing the ensuing causes (1) The coatings (TiC, Ti_3Al) contained undecomposed Ti_2AlC and its breakdown products, which might increase their hardness and abrasion resistance (Ref 51-53). Furthermore, because the Ti_2AlC particles and the matrix have a strong link, it is challenging to remove the Ti_2AlC particles from the matrix; (2) In certain circumstances, Ti_2AlC may develop a lubricating film on the surface of the coatings. The Ti_2AlC structure has weak links between the atomic layers of Al, Ti, and C. When the structure supported the GCr15 ball's normal load, it was simple to deform along the base plane's vertical axis. This raised the

Table 5 Element analyses of each point marked in Fig. 17 (at.%)

Point	Element composition			
	Ti	Al	C	O
A	55.33	6.34	1.15	37.18
B	67.17	8.42	15.31	9.10

dislocation slip energy, which led to lattice slip (Ref 54), and improved the coatings' capacity to reduce friction.

The phases observed in wear debris (A, B) were analyzed by EDS to confirm their elemental compositions (Table 5). Particularly, Ti, Al, C, and O elements made up a large portion of the wear debris (A, B), which confirmed its composition to be Ti_2AlC, Al_2O_3, and TiO_2 as identified by the XPS results. Such composition may be explained because Ti and Al elements were oxidized by the O elements from the environment, creating a soft and thin layer of oxide films under ambient temperature and friction. As a result, the primary wear mechanisms of the pure TC4 coating were abrasive wear, plastic deformation, and adhesive wear. The main processes for wear on coatings with Ti_2AlC additions, however, are mildly abrasive and oxidation. The exact mechanism of Ti_2AlC self-
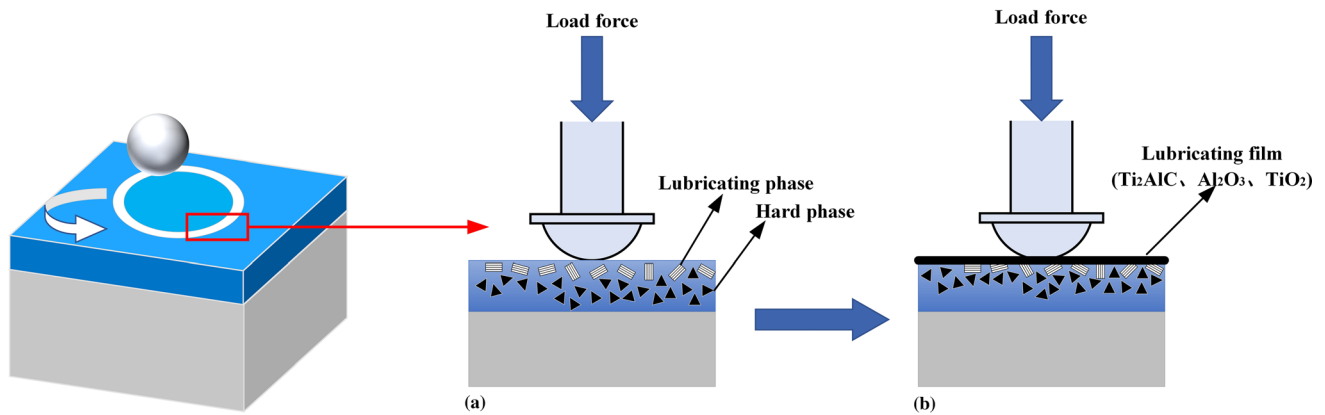
Fig. 18 The mechanism of Ti$_2$AlC self-lubrication coating

lubrication of the coating is described in Fig. 18. Firstly, the Ti$_2$AlC self-lubricating phase was uniformly distributed on the coating's top surface (Fig. 18a). Secondly, when the wear experiment started, the grinding ball started to contact the coating surface, and the Ti$_2$AlC solid-lubricating phase began to migrate to the coating surface. After that, since the Ti$_2$AlC phase had a small shear strength, it was sheared on the coating surface and spread to the contact surface due to pressure and friction, thereby forming a Ti$_2$AlC solid-lubricating film layer (Fig. 18b).

4. Conclusions

We used laser cladding to apply a TC4/Ti$_2$AlC composite coating to the Ti6Al4V substrate to increase the titanium alloy's wear resistance and lubricating capabilities. The microstructure, phase compositions, tribological performance, and wear mechanisms of the composite coatings were investigated, and the main conclusions can be summarized as follows:

1. By employing 5wt.%Ti$_2$AlC, 10wt.%Ti$_2$AlC, and 15wt.%Ti$_2$AlC and TC4 powder combinations, respectively, the defect-free and enriched self-lubricating Ti$_2$AlC composite coatings are effectively created by laser cladding on Ti6Al4V substrate.
2. As the content of Ti$_2$AlC increased from 0wt.% to 15wt.%, the average hardness of the composite coatings increased from 340.95 HV$_{0.5}$ to 388.91 HV$_{0.5}$. The distribution of TiC and Ti$_3$Al hard phases in dispersion, solid solution, and grain refinement strengthening are the major causes of the increase in hardness.
3. Compared with 5wt.% Ti$_2$AlC and 15wt.% Ti$_2$AlC coating, the surface of the coating enriched with massive self-lubricating phase Ti$_2$AlC, the TiO$_2$, and Al$_2$O$_3$ lubricating film, the 10wt.% Ti$_2$AlC coating had the lowest wear rate and friction coefficient due to the combination of TiC, Ti$_3$Al hard phases, and good toughness.
4. Even if the major wear mechanisms of the pure TC4 coating are said to be severe adhesion wear and oxidative wear due to self-lubricating phase Ti$_2$AlC, and TiO$_2$ and Al$_2$O$_3$ lubricating film during the wear process, the addition of Ti$_2$AlC composite coatings are primarily slight abrasive wear and oxidation wear.

Author Contributions

SH: investigation, Data curation, Writing original draft. MP: Conceptualization, Methodology, Formal analysis. JC: Supervision, Writing-review and editing. JZ: Investigation. F-QJ: Investigation.

Conflict of interest

The authors affirm that they have no known financial or interpersonal conflicts that would have seemed to impact the research presented in this study.

References

1. R.C. Fernandez, T. Tobie and J. Collazo, Increase wind Gearbox Power Density by Means of IGS (Improved Gear Surface), *Int. J. Fatigue*, 2022, **159**, p 106789. https://doi.org/10.1016/j.ijfatigue.2022.106789
2. T.M. Chen, C.C. Zhu, H.J. Liu, P.T. Wei, J.Z. Zhu and Y.Q. Xu, Simulation and Experiment of Carburized Gear Scuffing Under Oil Jet Lubrication, *Eng. Fail. Anal.*, 2022 https://doi.org/10.1016/j.engfailanal.2022.106406
3. A. Suresh, K.V.V. Sai Kalyan, K.S. Sibin Kumar, K. Vinod Kumar, V. Tanishka Varma and B. Sravan Kumar, Design and Simulation of Gear Box for Stone Crushing Ball Mill, *Mater. Today Proc.*, 2022 https://doi.org/10.1016/j.matpr.2022.04.456
4. L. Shi, X.F. Cui, J. Li, G. Jin, J.N. Liu and H.L. Tian, Improving the Wear Resistance of Heavy-Duty Gear Steels by Cyclic Carburizing, *Tribol. Int.*, 2022, **171**, p 107576. https://doi.org/10.1016/j.triboint.2022.107576
5. R.L. Dalcin, V.M.D. Menezes, L.F. Oliveira, C.H.D. Silva, J.C.K.D. Neves, C.A.T.S. Diehl and A.D.S. Rocha, Improvement on Pitting Wear Resistance of Gears by Controlled Forging and Plasma Nitriding, *J. Market. Res.*, 2022, **18**, p 4698–4713. https://doi.org/10.1016/j.jmrt.2022.04.122
6. V. Kharka, N.K. Jain and K. Gupta, Sustainability and Performance Assessment of Gear Hobbing Under Different Lubrication Environments for Manufacturing of 20MnCr5 Spur Gears, *Sustain. Mater. Technol.*, 2022, **31**, e00388. https://doi.org/10.1016/j.susmat.2022.e00388

7. Z.Y. Zhou, X.B. Liu, S.G. Zhuang, X.H. Yang, M. Wang and C.F. Sun, Preparation and High Temperature Tribological Properties of Laser In-Situ Synthesized self-Lubricating Composite Coatings Containing Metal Sulfides on Ti6Al4V alloy, *Appl. Surf. Sci.*, 2019, **481**, p 209–218. https://doi.org/10.1016/j.apsusc.2019.03.092

8. Y.Q. Zhao, Y. Han and Y. Xiao, An Asynchronous Dual-Frequency Induction Heating Process for Bevel Gears, *Appl. Therm. Eng.*, 2020, **169**, p 114981. https://doi.org/10.1016/j.applthermaleng.2020.114981

9. J.W. Zhang, W. Li, H.Q. Wang, Q.P. Song, L.T. Lu, W.J. Wang and Z.W. Liu, A Comparison of the Effects of Traditional Shot Peening and Micro-Shot Peening on the Scuffing Resistance of Carburized and Quenched Gear Steel, *Wear*, 2016, **368–369**, p 253–257. https://doi.org/10.1016/j.wear.2016.09.029

10. H.S. Gupta, M. Hussain, P.K. Singh, V. Kumar, S. Kumar and A.K. Das, Laser Surface Modification of SAE8620 HVD Material for Transmission Gear, *Mater. Today Proc.*, 2019, **11**, p 813–817. https://doi.org/10.1016/j.matpr.2019.03.047

11. M. Fan, R.L. Sun and H. Wang, Quality Analysis of Ni_{60}/Ni/MoS_2 Self-Lubricating Composite Coating on TC4 Surface by Laser Cladding, *Hot Work. Technol.*, 2016, **45**(12), p 123–126. https://doi.org/10.14158/j.cnki.1001-3814.2016.12.037

12. P. Wang and Y.S. Ye, Solid Self-Lubricating Coatings on TC4 Titanium Alloy by Laser Cladding with h-BN, *Surf. Technol.*, 2015, **44**(08), p 44–48. https://doi.org/10.16490/j.cnki.issn.1001-3660.2015.08.008

13. J. Xu, W.J. Liu and M.L. Zhong, Microstructure and Dry Sliding Wear Behavior of MoS_2/TiC/Ni Composite Coatings Prepared by Laser Cladding, *Surf. Coat. Technol.*, 2006, **200**, p 4227–4232. https://doi.org/10.1016/j.surfcoat.2005.01.036

14. M.S. Yang, X.B. Liu, J.W. Fan, X.M. He, S.H. Shi, G.Y. Fu, M.D. Wang and S.F. Chen, Microstructure and Wear Behaviors of Laser Clad NiCr/Cr_3C_2–WS_2 High Temperature Self-Lubricating Wear-Resistant Composite Coating, *Appl. Surf. Sci.*, 2012, **258**(37), p 57–3762. https://doi.org/10.1016/j.apsusc.2011.12.021

15. B. Podgornik, T. Kosec, A. Kocijan and Č Donik, Tribological Behavior and Lubrication Performance Of Hexagonal Boron Nitride (h-BN) as a Replacement for Graphite in Aluminium Forming, *Tribol. Int.*, 2015, **81**, p 267–275. https://doi.org/10.1016/j.triboint.2014.09.011

16. H. Torres, S. Slawik, C. Gachot, B. Prakash and M. Rodríguez Ripoll, Microstructural Design of Self-Lubricating Laser Claddings for Use in High Temperature Sliding Applications, *Surf. Coat. Technol.*, 2018, **337**, p 24–34. https://doi.org/10.1016/j.surfcoat.2017.12.060

17. A.K. Das, Effect of Solid Lubricant Addition in Coating Produced by Laser Cladding Process: A Review, *Mater. Today Proc.*, 2022, **56**, p 1274–1280. https://doi.org/10.1016/j.matpr.2021.11.217

18. H. Torres, T. Vuchkov, S. Slawik, C. Gachot, B. Prakash and M. Rodríguez Ripoll, Self-Lubricating Laser Claddings for Reducing Friction and Wear from Room Temperature to 600 °C, *Wear*, 2018, **408**, p 22–23. https://doi.org/10.1016/j.wear.2018.05.001

19. M.M. Quazi, M.A. Fazal, A.S.M.A. Haseeb, F. Yusof, H.H. Masjuki and A. Arslan, A Review to the Laser Cladding of Self-Lubricating Composite Coatings, *Lasers Manuf. Mater. Process.*, 2016, **3**, p 67–99. https://doi.org/10.1007/s40516-016-0025-8

20. G.M. Song, Y.T. Pei, W.G. Sloof, S.B. Li, J.T.M. Hosson and S. van der Zwaag, Oxidation-Induced Crack Healing in Ti_3AlC_2 Ceramics, *Scr. Mater.*, 2008, **58**, p 13–16. https://doi.org/10.1016/j.scriptamat.2007.09.006

21. A.S. Farle, C. Kwakernaak, S. van der Zwaag and W.G. Sloof, A Conceptual Study into the Potential of $M_{n+1}AX_n$-Phase Ceramics for Self-Healing of Crack Damage, *J. Eur. Ceram. Soc.*, 2015, **35**, p 37–45. https://doi.org/10.1016/j.jeurceramsoc.2014.08.046

22. S. Li, G. Song, K. Kwakernaak, S. van der Zwaag and W.G. Sloof, Multiple Crack Healing of a Ti_2AlC Ceramic, *J. Eur. Ceram. Soc.*, 2012, **32**, p 1813–1820. https://doi.org/10.1016/j.jeurceramsoc.2012.01.017

23. H.J. Yang, Y.T. Pei and J.T.M. Hosson, Oxide-Scale Growth on Cr_2AlC Ceramic and its Consequence for Self-Healing, *Scr. Mater.*, 2013, **69**, p 203–206. https://doi.org/10.1016/j.scriptamat.2013.04.013

24. Z. Feng, P. Ke, Q. Huang and A. Wang, The Scaling Behavior and Mechanism of Ti_2AlC MAX Phase Coatings in Air and Pure Water Vapor, *Surf. Coat. Technol.*, 2015, **272**, p 380–386. https://doi.org/10.1016/j.surfcoat.2015.03.037

25. J. Cao, Z.W. Yin, H.L. Li, G.Y. Gao and X.L. Zhang, Tribological and Mechanical Properties of Ti_2AlC Coating at Room Temperature and

800°C, *Ceram. Int.*, 2018, **44**, p 1046–1051. https://doi.org/10.1016/j.ceramint.2017.10.045

26. M.W. Barsoum, The $M_{N+1}AX_N$ Phases: A New Class of Solids: Thermodynamically Stable Nanolaminates, *Prog. Solid State Chem.*, 2000, **28**, p 201–281. https://doi.org/10.1016/S0079-6786(00)00006-6

27. M. Magnuson and M. Mattesini, Chemical Bonding and Electronic-Structure in MAX Phases as Viewed by X-ray Spectroscopy and Density Functional Theory, *Thin Solid Films*, 2017, **621**, p 108–130. https://doi.org/10.1016/j.tsf.2016.11.005

28. P. Eklund, M. Beckers, U. Jansson, H. Hogberg and L. Hultman, The $M_{n+1}AX_n$ Phases: Materials Science and Thin-Film Processing, *Thin Solid Films*, 2010, **518**, p 1851–1878. https://doi.org/10.1016/j.tsf.2009.07.184

29. M.W. Qureshi, X.X. Ma, X.H. Zhang, G.Z. Tang, R. Paudel and D. Paudyal, Ab-Initio Predictions of Phase Stability, Electronic Structure, and Optical Properties of (0001)-MAXsurfaces in M_2AC (M = Cr, Zr, Hf; A = Al, Ga), *J. Phys. Chem. Solids*, 2022, **160**, p 110338. https://doi.org/10.1016/j.jpcs.2021.110338

30. N. Goossens, B. Tunca, T. Lapauw, K. Lambrinou, J. Vleugels, in *MAX Phases, Structure, Processing, and Properties*, ed. by M. Pomeroy. Encyclopedia of Materials: Technical Ceramics and Glasses, (Elsevier, 2021), pp. 182–199. https://doi.org/10.1016/B978-0-12-818542-1.00015-1

31. J.L. Smialek, Environmental resistance of a Ti_2AlC-type MAX Phase in a High Pressure Burner Rig, *J. Eur. Ceram. Soc.*, 2017, **37**, p 23–34. https://doi.org/10.1016/j.jeurceramsoc.2016.07.038

32. Y. Xiao, H.Q. Xiao, J.Y. Feng, B. Lin and Y. Wang, Core-shell ZrC/Ti_2AlC Reinforced Composite Coatings Prepared by Laser Cladding on Zr-Alloy Substrates, *Ceram. Int.*, 2022, **48**(6), p 8136–8142. https://doi.org/10.1016/j.ceramint.2021.12.016

33. Q.Y. Tan, W.M. Zhuang, M. Attia, R. Djugum and M.X. Zhang, Recent Progress in Additive Manufacturing of Bulk MAX Phase Components: A Review, *J. Mater. Sci. Technol.*, 2022, **131**, p 30–47. https://doi.org/10.1016/j.jmst.2022.05.026

34. X.J. Li, S.H. Wang, G.X. Wu, D.P. Zhou, J.B. Pu, M. Yu, Q. Wang and Q.S. Sun, Oxidation and Hot Corrosion Behaviors of MAX-Phase Ti_3SiC_2, Ti_2AlC, Cr_2AlC, *Ceram. Int.*, 2022 https://doi.org/10.1016/j.ceramint.2022.05.356

35. Y. Zhu, X.B. Liu, Y.F. Liu, G. Wang, Y. Wang, Y. Meng and J. Liang, Development and Characterization of Co-Cu/Ti_3SiC_2 Self-Lubricating Wear Resistant Composite Coatings onTi6Al4V Alloy by Laser Cladding, *Surf. Coat. Technol.*, 2021, **424**, p 127664. https://doi.org/10.1016/j.surfcoat.2021.127664

36. P. Richardson, D. Cuskelly, M. Brandt and E. Kisi, Microstructural Analysis of In-Situ Reacted Ti_2AlC MAX Phase Composite Coating by Laser Cladding, *Surf. Coat. Technol.*, 2020, **385**, p 125360. https://doi.org/10.1016/j.surfcoat.2020.125360

37. M. Das, S. Bysakh, D. Basu, T.S.S. Kumar, V.K. Balla, S. Bose and A. Bandyopadhyay, Microstructure, Mechanical and Wear Properties of Laser Processed SIC Particle Reinforced Coatings on Titanium, *Surf. Coat. Technol.*, 2011, **205**, p 4366–4373. https://doi.org/10.1016/j.surfcoat.2011.03.027

38. X. Lei and N. Lin, Structure and Synthesis of MAX Phase Materials: A Brief Review, *Crit. Rev. Solid State Mater. Sci.*, 2021 https://doi.org/10.1080/10408436.2021.1966384

39. T.T. Ai, Q.F. Niu, Z.F. Deng, W.H. Li, H.F. Dong, R. Jing and X.Y. Zou, Nature-Inspired Nacre-Like Ti_6Al_4V-(Ti_2AlC/TiAl) Laminate Composites Combining Appropriate Strengthand Toughness with Synergy Effects, *Intermetallics*, 2020, **121**, p 106774. https://doi.org/10.1016/j.intermet.2020.106774

40. H. Zhang, C.H. Zhang, Q. Wang, C.L. Wu, S. Zhang, J. Chen and A.O. Abdullah, Effect of Ni Content on Stainless Steel Fabricated by Laser Melting Deposition, *Opt. Laser Technol.*, 2018, **101**, p 363–371. https://doi.org/10.1016/j.optlastec.2017.11.032

41. G.R. Xu, X.S. Guan, Y.L. Qiao and Y. Gao, Analysis and Innovation for Penetrant Testing for Airplane Parts, *Proc. Eng.*, 2015, **99**, p 1438–1442. https://doi.org/10.1016/j.proeng.2014.12.681

42. J.H. Ye and D.L. Hu, *Utility Inorganic Materials Thermodynamics Data Handbook*, 2nd ed. Metallurgy Industry Press, Beijing, 2002

43. J. Li, Z.S. Yu and H.P. Wang, Wear behaviors of an (TiB+TiC)/Ti Composite Coating Fabricated on Ti6Al4V by Laser Cladding, *Thin Solid Films*, 2011, **519**(15), p 4804–4808. https://doi.org/10.1016/j.tsf.2011.01.034

44. B. He, L.J. Zhang, Q.H. Zhu, J. Wang, X. Yun, J.S. Luo and Z.K. Chen, Effect of Solution Treated 316L Layer Fabricated by Laser Cladding on Wear and Corrosive Wear Resistance, *Opt. Laser Technol.*, 2020, **121**, p 105788. https://doi.org/10.1016/j.optlastec.2019.105788

45. B.X. Song, T.B. Yu, X.G. Jiang, W.C. Xi and X.L. Lin, The Relationship Between Convection Mechanism and Solidification Structure of the Iron-Based Molten Pool in Metal Laser Direct Deposition, *Int. J. Mech. Sci.*, 2020, **165**, p 105207. https://doi.org/10.1016/j.ijmecsci.2019.105207

46. A. Khorram, A.D. Jamaloei, A. Jafari, M. Paidar and X.J. Cao, Microstructural Evolution of Laser-Clad $75Cr_3C_2+25(80Ni_{20}Cr)$ Powder on Inconel 718 Superalloy, *J. Mater. Process. Technol.*, 2020, **284**, p 116735. https://doi.org/10.1016/j.jmatprotec.2020.116735

47. R. Benitez, W.H. Kan, H. Gao, M. O'Neal, G. Proust, A. Srivastava and M. Radovic, Mechanical Properties and Microstructure Evolution of $Ti2AlC$ Under Compression in 25–1100 °C Temperature Range, *Acta Mater.*, 2020, **189**, p 154–165. https://doi.org/10.1016/j.actamat.2020.02.057

48. Y. Wang, X.B. Liu, Y.F. Liu, Y.S. Luo and Y. Meng, Microstructure and Tribological Performance of Ni60-Based Composite Coatings on Ti6Al4V Alloy with Different Ti_3SiC_2 Ceramic Additions by Laser Cladding, *Ceram. Int.*, 2020, **46**(18), p 28996–29010. https://doi.org/10.1016/j.ceramint.2020.08.071

49. Z.Y. Wang, G.S. Ma, Z.C. Li, H.T. Ruan, J.G. Yuan, L. Wang, P.L. Ke and A.Y. Wang, Corrosion Mechanism of Ti_2AlC MAX Phase Coatings Under the Synergistic Effects of Water Vapor and Solid NaCl at 600 °C, *Corros. Sci.*, 2021, **192**, p 109788. https://doi.org/10.1016/j.corsci.2021.109788

50. H.X. Liu, X.W. Zhang, Y.H. Jiang and R. Zhou, Microstructure and High Temperature Oxidation Resistance of In-Situ Synthesized TiN/Ti_3Al Intermetallic Composite Coatings on Ti6Al4V Alloy by Laser Cladding Process, *J. Alloy. Compd.*, 2016, **670**, p 268–274. https://doi.org/10.1016/j.jallcom.2015.10.168

51. S. Saroj, C.K. Sahoo, D. Tijo, K. Kumar and M. Masanta, Sliding Abrasive Wear Characteristic of TIG Cladded TiC Reinforced Inconel825 Composite Coating, *Int. J. Refract. Metals Hard Mater.*, 2017 https://doi.org/10.1016/j.ijrmhm.2017.08.005

52. X. Zhao, L.Y. Duan and Y.G. Wang, Improved Shear Strength of SiC-coated 3DC/SiC Composite Joints with a Tailored Ti-Si-C Interlayer, *J. Eur. Ceram. Soc.*, 2019, **39**(4), p 788–797. https://doi.org/10.1016/j.jeurceramsoc.2018.11.016

53. A. Bansal, D.K. Goyal, P. Singh, A.K. Singla, M.K. Gupta, N. Bala, J. Kolte and G. Setia, Erosive Wear Behavior of HVOF-Sprayed Ni-$20Cr_2O_3$ Coating on Pipeline Materials, *Int. J. Refract Metal Hard Mater.*, 2020, **92**, p 105332. https://doi.org/10.1016/j.ijrmhm.2020.105332

54. X. Li, C.H. Zhang, S. Zhang, C.L. Wu, Y. Liu, J.B. Zhang and M. Babar Shahzad, Manufacturing of Ti_3SiC_2 Lubricated Co-Based Alloy Coatings Using Laser Cladding Technology, *Opt. Laser Technol.*, 2019, **114**, p 209–215. https://doi.org/10.1016/j.optlastec.2019.02.001